

A General-Purpose Neuromorphic Sensor based on Spiketrum Algorithm: Hardware Details and Real-life Applications

MHD Anas Alsakkal, Runze Wang, Jayawan Wijekoon, and Piotr Dudek, *Member, IEEE*

Abstract— Spiking Neural Networks (SNNs) offer a biologically inspired computational paradigm, enabling energy-efficient data processing through spike-based information transmission. Despite notable advancements in hardware for SNNs, spike encoding has largely remained software-dependent, limiting efficiency. This paper addresses the need for adaptable and resource-efficient spike encoding hardware by presenting an area-optimized hardware implementation of the Spiketrum algorithm, which encodes time-varying analogue signals into spatiotemporal spike patterns. Unlike earlier performance-optimized designs, which prioritize speed, our approach focuses on reducing hardware footprint, achieving a 52% reduction in Block RAMs (BRAMs), 31% fewer Digital Signal Processing (DSP) slices, and a 6% decrease in Look-Up Tables (LUTs). The proposed implementation has been verified on an FPGA and successfully integrated into an IC using TSMC180 technology. Experimental results demonstrate the system's effectiveness in real-world applications, including sound and ECG classification. This work highlights the trade-offs between performance and resource efficiency, offering a flexible, scalable solution for neuromorphic systems in power-sensitive applications like cochlear implants and neural devices.

Index Terms— Neuromorphic Sensor, hardware encoder, FPGA implementation, spike encoding, sound classification, ECG classification.

I. INTRODUCTION

Brain-inspired computation has paved the way for revolutionary advancements in the form of Spiking Neural Networks (SNNs). SNNs have garnered considerable attention due to their brain-inspired architecture and energy-efficient computational paradigms [1]. Unlike conventional neural networks, SNNs adopt a unique approach to data processing, relying on spikes to convey information. These spikes, devoid of inherent values, leverage their spatio-temporal relationships to effectively transmit processed data. However, the translation of external data into these spikes, known as spike encoding, has primarily remained a software-driven process [2]. The evolution of hardware spike-based processors over the last decade has been noteworthy. Despite these advancements, encoding strategies have largely relied on conventional processing methods, limiting the potential efficiency gains offered by dedicated hardware [2].

While specialized spike encoding hardware exists, its rigid implementation often confines it to a single encoding scheme, lacking the adaptability required for dynamic reconfiguration [3-5]. Bohte et al., utilizes temporal population coding to chronologically encode input data [6], whereas, Mostafa, applied temporal encoding for the classification of an MNIST dataset featuring hand-written digit images [9]. On the other hand, rate encoding has been harnessed by Liu et al., Querlioz et al., and Bagheri et al. for the recognition of images containing digits [7-9]. The efficacy of SNNs in real-world applications is intricately tied to the chosen spike encoding scheme [10]. Therefore, this limitation underscores the need for a more versatile and adaptable spike encoding approach.

Designing neuromorphic architectures with mimicking low-level details of complex biological sensory systems could provide an understanding of techniques used by the biological system. However, implementing such architectures in hardware may not be power and resources efficient. Therefore, introducing a higher level of abstraction in the cochlear model, while maintaining the ability to design and implement the model in the latest low-power electronic technologies, could provide more power-efficient, compact and stable sensor for computing machines and neural implantable devices. The algorithm of Spiketrum [11] is designed to characterize and convert time-varying analogue signals into highly efficient spatiotemporal spike patterns. It offers a sparse and efficient coding scheme, allowing precise control over spike rates.

In earlier research [12], we introduced a “performance-optimized” methodology for implementing Spiketrum, which emphasizes processing speed by harnessing additional resources to alleviate computational burdens. This approach is particularly well-suited for real-time FPGA deployment, excelling in managing demanding computational tasks and delivering significant performance enhancements, making it ideal for scenarios requiring high-fidelity input representation with heightened spike rates. Nevertheless, this implementation may not be appropriate for applications where factors such as power consumption and hardware footprint are paramount, as seen in cochlear implants, for example. Thus, in this work, we present an “area-optimized” hardware implementation of Spiketrum, focused on conserving hardware resources and minimizing the overall implementation footprint. Our area-optimized solution demonstrates a noteworthy reduction: a 52% decrease in Block RAMs (BRAMs), 31% fewer Digital Signal Processing (DSP) slices, and a 6% decline in Look-Up Tables (LUTs), in comparison to the “performance-optimized” approach. Furthermore, we conducted FPGA-based

Manuscript received Jan XX, 2025; revised Mar XX, 2025; accepted Mar XX, 2025. Date of publication Apr XX, 2025; date of current version Apr XX, 2025. The authors are with the Department of Electrical and Electronic Engineering, The University of Manchester, Manchester, UK. Corresponding author Jayawan Wijekoon (e-mail: jayawan.wijekoon@manchester.ac.uk). Color versions of one or more of the figures in this article are available online at <http://ieeexplore.ieee.org>.

> REPLACE THIS LINE WITH YOUR MANUSCRIPT ID NUMBER (DOUBLE-CLICK HERE TO EDIT) <

verification of the proposed area-optimized hardware design and successfully transformed it into an Integrated Circuit (IC) using the TSMC180 Technology. Our findings include FPGA-based verification results and a demonstration of various real-life applications, such as EMG, sound, and ECG classification, showcasing the efficacy and versatility of our approach.

This paper is organized as follows: Chapter II introduces the Spiketrum algorithm and provides detailed insights into its proposed FPGA-based hardware implementation. Chapter III describes the chip implementation of Spiketrum. Chapter IV details the methodologies employed to evaluate the proposed FPGA-based implementation of Spiketrum. Chapter V presents experimental results and demonstrates real-life classification-based applications. Chapter VI discusses the trade-offs between performance- and area-optimized implementations, comparing them with recent works in literature. Finally, conclusions are drawn in Chapter VII.

II. SPIKETRUM: DESIGN CONSIDERATIONS AND IMPLEMENTATION DETAILS

In this chapter, we delve into the intricacies of the FPGA-based implementation of Spiketrum, shedding light on its design considerations and implementation specifics. We particularly focus on the proposed architecture of the area-optimized approach and elucidate its distinctions from our previous work performance-optimized implementation [12]. Opting for an FPGA-based implementation is strategic, as it aligns closely with the specific requirement for configurability. This choice empowers users to finely tune spike rates, effectively striking a balance between output quality and power consumption. The proposed hardware architecture is based on three fundamental stages: Feature Extraction, Residual Computing, and Intensity-to-Place Coding, as can be seen in Fig. 1-a.

Within the Feature Extraction stage, the incoming signal undergoes transformation via a matching pursuit signal decomposition method [13], utilizing a predetermined dictionary comprising 40 Gammatone kernels. The process of selecting the most suitable kernel for the observed segment of the input signal is achieved through convolution operations. This procedure yields intricate codes that encapsulate spatial position denoted as ' m_i ', precise temporal positioning denoted as ' τ_i ', and the convolution intensity denoted as ' s_i '.

These codes characterize the correspondence between the signal and the selected Gammatone kernel. It's crucial to emphasize that each code (m_i , τ_i , s_i) serves as an effective repository of the unique attributes inherent to the input signal, ensuring the preservation of distinguished features.

To facilitate real-time processing, Spiketrum segments input signals. Each processed segment generates a configurable number of spikes per segment (sps). An illustration of signal encoding and the resulting code generation from the hardware implementation is presented in Fig. 1-b. The input signal consists of two segments (Fig. 1-b (i)), representing a Cymbal tone sourced from the Medley dataset [14], sampled at 16 kHz, and encoded at a spike rate of 1000 sps. The resulting codes are depicted in Fig. 1-b (ii),

where the x-axis represents the time shift of the code (τ_i), the y-axis represents the kernel index of the code (m_i), and the size of each dot represents the code's intensity (s_i). This visual representation offers insight into the temporal and spatial distribution of spikes generated during signal processing.

The iterative nature of the algorithm highlights its emphasis on encoding significant features first, followed by processing less pivotal ones. This iterative process involves removing the previously encoded kernel component from the current input segment before generating a new code. The Residual Computing unit serves a pivotal role in selectively obliterating the influence of already captured features. This ensures the representational distinctiveness of each code in relation to the auditory signal, allowing for the precise extraction and preservation of essential information.

In the Intensity-to-Place (ITP) coding stage, the generated codes undergo a mapping process, culminating in binary spike trains on output channels (Fig. 1-b (iii)). This stage is meticulously crafted to minimize any loss of information during the transition from continuous waveforms to discrete spikes. By preserving the essential features encoded in the generated codes, this stage ensures fidelity in the representation of the input signal's characteristics within the binary spike trains.

The proposed neuromorphic sensor is realized on the XEM7310 Opal Kelly board, which boasts a Xilinx Artix-7 FPGA, as illustrated in Fig. 1-c. This board is equipped with a range of essential peripherals, including SDRAMs, EEPROMs, and clock generators, enhancing its versatility and usability. In order to enable real-time processing, segments of input sensory signals are captured, sent to the FPGA, through a high-speed USB 3 interface, for spike generation. Additionally, to support live processing of audio signals, the device incorporates auxiliary microphone circuits, further expanding its capabilities and applicability. The output spikes generated by the neuromorphic sensor are conveniently accessible through a USB-C port. This port design not only facilitates efficient post-sensing processing but also allows for seamless integration of the sensor with larger, more complex neuromorphic systems. This integration is achieved through direct hardware device connection and configuration of communication protocols, such as the Address-Event Representation (AER).

The neuromorphic sensor is designed with flexible power supply options, allowing it to be powered either through a USB 3 port or a standard 5V DC charger. During real-time processing at a frequency of 200 MHz, the device consumes a total power of 382 mW, encompassing both static and dynamic power requirements. Fig. 1-d provides a breakdown of dynamic power consumption, which constitutes 89% of the total power draw when operating at maximum speed, along with the utilized hardware resources on the FPGA. To estimate power consumption and hardware utilization, we relied on Xilinx Vivado tools [15], as direct measurements on the FPGA are impractical.

Furthermore, to enhance the precision of the proposed implementation while maintaining low power usage, we strategically employ a 34-bit fixed-point architecture for data

> REPLACE THIS LINE WITH YOUR MANUSCRIPT ID NUMBER (DOUBLE-CLICK HERE TO EDIT) <

processing. Fixed-point architectures are known for offering power-optimized solutions, emphasizing efficiency and low power consumption [16]. In contrast, floating-point architectures excel in performance optimization, prioritizing computational accuracy. However, in our approach, we strike a balance by utilizing a high bit resolution within the fixed-

point architecture. This allows us to combine the power efficiency of fixed-point with precision that approaches the capabilities of floating-point solutions.

Moreover, to achieve optimal resource utilization, all on-chip memories are outfitted with a Native interface, chosen over AXI4 interface to mitigate FPGA slice usage.

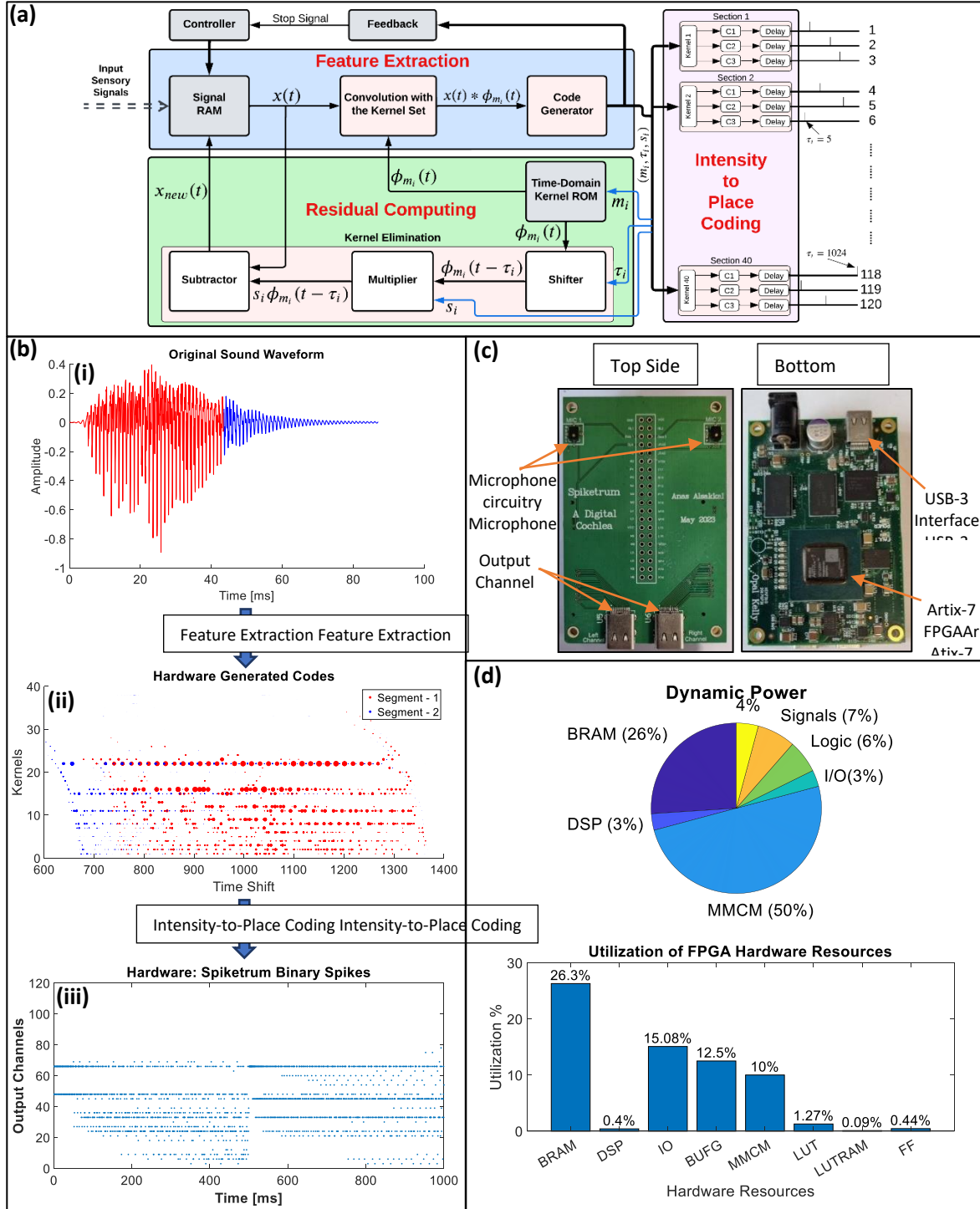


Fig. 1: The proposed FPGA-based neuromorphic cochlea employs the Spiketrum spike-encoding algorithm. (a) shows the hardware architecture, where Feature Extraction processes audio signals and generates codes through Residual Computing, which are converted into spikes via Intensity-to-Place Coding. (b) presents the output for a two-segment audio signal at 1000 spikes per second (sps). (c) illustrates the real-time FPGA prototype, allowing live audio input via a microphone or USB-3, with 120 spiking channels available through a USB-C interface. (d) details power consumption (1.382 W at 200 MHz) and resource utilization, including Block RAM tiles (BRAM), Digital Signal Processing slices (DSP), Input/output (IO), Buffer Global Clock (BUFG), Mixed-Mode Clock Manager (MMCM), Lookup tables (LUT), LUT RAMs, and Flip-Flops (FF).

> REPLACE THIS LINE WITH YOUR MANUSCRIPT ID NUMBER (DOUBLE-CLICK HERE TO EDIT) <

These memories are generated utilizing the Xilinx Block Memory Generator (BMG) IP Core, employing the Minimum Area Algorithm to minimize the number of required block memory primitives. This strategic approach ensures efficient utilization of on-chip resources, enhancing the overall performance and scalability of the hardware implementation.

The adapted Matching Pursuit (MP) algorithm [13] decomposes any signal into a linear expansion of shifted and scaled waveforms (kernel set). Conventionally, convolution is used to identify the most suitable kernels for the observed input signal segment. In the translation of the Feature Extraction process into hardware architecture, two distinct approaches were explored. These approaches were selected to strike a balance between different optimization goals and to cater to varying application needs.

The first approach, known as the “performance-optimized” strategy, prioritizes processing speed and efficiency by leveraging enhanced parallel processing capabilities. Operating at a clock speed of 200 MHz, it can generate up to 80 spikes per segment (sps), equivalent to 1,840 spikes per second. This renders it highly suitable for applications requiring real-time, high-precision processing, such as autonomous vehicles or brain-computer interfaces (BCIs), where accurate data processing is essential for optimal performance. An FPGA-based implementation of the performance-optimized approach was detailed in [12], including verification results and demonstrations of its efficacy in audio processing applications.

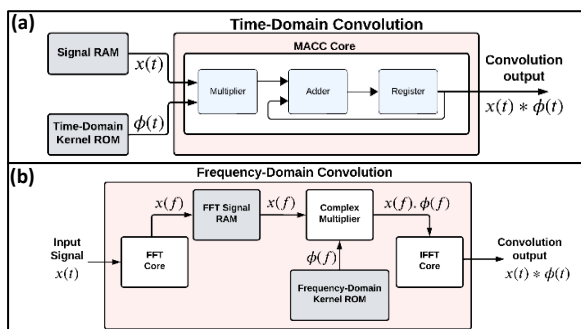


Fig. 2: A block diagram illustrates the proposed time-domain and frequency-domain implementations of the Convolution operation. (a) Time-domain convolution is implemented using a single DSP slice that performs multiply and accumulate (MACC) operation. (b) Fast Fourier Transform (FFT) of the input signal $x(t)$ is taken by the FFT Core and the results are stored on the FFT Signal RAM. Complex multiplication is performed between the computed FFT of the input signal $x(f)$ and the stored FFT values of the kernel set $\phi(f)$. Finally, the time domain convolution output is obtained by taking the inverse FFT (IFFT) of the result of the complex multiplication. More details on the frequency-domain based implementation can be found in [12].

On the other hand, the second approach, termed the “area-optimized” strategy, places emphasis on conserving hardware resources and minimizing the overall implementation footprint, even at the expense of some performance trade-offs. In this setup, convolution operations are executed sequentially in the time domain to determine the optimal

matching kernels for the processed segment of the signal. This involves utilizing a single DSP slice for multiplication and accumulation (MACC) operations, ensuring efficient resource utilization (Fig. 2-a). Operating at the maximum clock speed of 200 MHz, this approach achieves a spike rate of 16 spikes per segment (equivalent to 115 spikes per second). While real-time processing with low spike rates is feasible, the primary objective of this approach is to create a compact implementation suitable for low-cost FPGA-based setups or integration into low silicon area integrated circuits (ICs). This approach results in significantly lower resource utilization, including a 52% decrease in Block RAMs (BRAMs), 31% fewer Digital Signal Processing (DSP) slices, and a 6% decline in Look-Up Tables (LUTs), culminating in a substantial area reduction. Moreover, it achieves approximately 75% power savings, making it an ideal choice for applications where power consumption and hardware footprint are critical considerations, such as cochlear implants.

In the subsequent sections, we delve into the hardware intricacies and methodologies employed within the three primary stages of the proposed implementation. Special emphasis is placed on delineating where the area-optimized solution diverges from the performance-optimized approach. By scrutinizing these distinctions, our goal is to furnish Spiketrum users with a comprehensive understanding of the design choices. This knowledge empowers users to make informed decisions and select the most suitable implementation for their diverse applications. Whether prioritizing performance optimization or area efficiency, understanding these nuances ensures the optimal utilization of Spiketrum across a range of real-world scenarios.

A. Feature Extraction

Continuous incoming audio segments are captured at the input and stored on the Signal RAM, which is a single-port RAM with storage capacity of 8.7 kB (Fig. 1-a). The Signal RAM is used to hold both captured segments and consecutive residuals. The operational cycle of the Signal RAM is overseen by a custom controller, responsible for coordinating the read and write operations to and from the Signal RAM. In addition, the controller manages the transfer of new data to the MACC core for subsequent convolution operations. After capturing a new sound segment, the controller verifies the readiness of the MACC core to process the new segment. If the MACC core is idle and prepared for the new data influx, the controller triggers a hand-shaking protocol that enables the simultaneous transfer of data to the MACC core.

The Code Generator analyses the continuous output from the MACC core to identify the maximum convolution intensity s_i . Once the MACC core operation concludes, the Code Generator retrieves the maximum convolution intensity s_i along with its coordinates - kernel index m_i and time shift τ_i . This is achieved using a 34-bit comparator that sequentially compares convolution intensities, updating the stored maximum convolution intensity s_i , kernel index m_i , and time shift τ_i . Upon completion of the convolution, the Code Generator dispatches the generated code (m_i, τ_i, s_i) to the Residual Computing and the Spike Generator processes.

> REPLACE THIS LINE WITH YOUR MANUSCRIPT ID NUMBER (DOUBLE-CLICK HERE TO EDIT) <

After removing the detected code from the original signal using the Residual Computing unit, the residue $x(t)_{new}$ is stored in the Signal RAM to extract the next dominant feature of the currently processed segment. The process of identifying subsequent matching kernels is repeated for a predetermined number of iterations per segment (k), resulting in a code set represented as:

$$S = [(m_1, \tau_1, s_1), (m_2, \tau_2, s_2), \dots, (m_k, \tau_k, s_k)] \quad (6.1)$$

Every code (m_i, τ_i, s_i) within the code set S represents a small sound waveform occurring at the temporal location τ_i with the shape of kernel m_i and amplitude s_i . The error $\epsilon(t)$ decreases as the number of generated codes, k , increases. The original waveform can be reconstructed by linearly superposing all small waveforms represented by the code set S . The amount of information loss depends on the nature of the selected kernel set as well as the number of generated codes, k .

The Feedback module evaluates the latest generated code and instructs the Controller to either initiate a new code generation process or conclude the encoding procedure. Our implementation integrates a straightforward halting mechanism that enables the encoder to cease encoding features when the convolution intensities of the captured features fall below a predefined threshold. By disregarding less significant features, this method minimizes resource usage and power consumption, thereby promoting a more cost-effective and streamlined encoding process. The Feedback module is implemented using a single comparator that compares the intensity of the generated code s_i with the predefined threshold.

B. Residual Computing

Spiketrum iteratively generates successive codes that encapsulate Gammatone patterns and features of captured sensory signals. This iterative process prioritizes the encoding of dominant features, while less significant features are processed subsequently, reflecting their relative importance. Achieving this entails eliminating the most recently encoded kernel component from the input segment before generating a new code. The Residual Computing unit facilitates this process by comprising three subunits: the Shifter, Multiplier, and Subtractor, as illustrated in Fig. 1-a.

To eliminate the kernel component from the currently processed segment, we employ a multi-step process. Firstly, the time-domain (T-D) values of the corresponding kernel, denoted as ϕ_{m_i} , are retrieved from the T-D Kernel ROM and transferred to the Shifter unit. The T-D Kernel ROM is a single-port ROM with a storage capacity of 346 kB. Since performing shifting operations using logic circuits for large segments can be challenging, we opt for a RAM-based approach.

The RAM adjusts its starting address dynamically based on the time shift value τ_i , which represents the maximum shift of the kernel centre. The maximum τ_i is ± 1024 , corresponding to half the segment size of 2048. During shifts, read operations always target addresses within the range of 1024 to 3072, irrespective of the specific τ_i . For positive τ_i , the starting address exceeds 1024, resulting in a logical right shift. For negative τ_i , the address is below 1024, causing a

logical left shift. After each read, the RAM resets to prepare for the next operation. The 13 kB Shifter RAM efficiently handles these processes, preserving the original kernel data.

After the shifting process, the shifted kernel is forwarded to a Multiplier unit, where it is scaled by the intensity of the captured code s_i . Real (non-complex) multiplication is executed using a single DSP48E1 Slice, renowned for its low-power consumption and capacity to handle 25×18 two's-complement multiplications [17]. To ensure proper timing and meet timing prerequisites, both the input and output buses of the Multiplier are pipelined at three stages. The resulting output from the Multiplier is then directed to the Subtractor unit. Here, the shifted scaled kernel $s_k \phi_{m_k}(t - \tau_k)$ is subtracted from the current input segment $x(t)$. The updated segment $x(t)_{new}$ is written back to the Signal RAM to process and generate a new code representing the next significant feature. The Subtractor unit is implemented using logic fabric on the FPGA, as the timing requirements for this simple operation can be easily met.

C. Intensity-to-Place Coding

Upon completing the Feature Extraction process, the Intensity-to-Place Coding scheme maps the generated codes to their corresponding output channels (Fig. 1-a). Each kernel is linked to a specific number N of output channels, also known as output fibres, which correspond to distinct intensity levels or firing thresholds. Based on statistical analyses presented in [11], the optimal number of output channels per kernel N that ensures high encoding sparsity while maintaining practical resource utilization has been determined to be three. These three output channels are characterized by logarithmically distributed center intensities, denoted as C_i (0.0065, 0.4115, and 25.8744). Since each of the 40 implemented kernels has three associated output channels, the total number of output channels in Spiketrum amounts to 120. In certain applications, however, the exact logarithmically distributed centre intensities for these three channels can be approximated or rounded to reduce the hardware precision required for computations. This adjustment can help optimize resource usage—particularly in low-power or constrained environments—while still preserving adequate encoding performance. The choice of how closely to approximate the centre intensities ultimately depends on the specific accuracy requirements and computational constraints of the target application.

The Spike Generator receives the generated code (m_i, τ_i, s_i) from the Code Generator and identifies the channel intensity C_i that closely corresponds to the code's intensity s_i . This determination is made from the three channels associated with the m_i kernel. Once the closest channel intensity is identified, the Spike Generator, adhering to the Intensity-to-Place scheme, waits for a time delay equal to the time shift τ_i . Subsequently, it emits a spike at the output channel with the code's kernel index m_i and the closest intensity level.

III. SPIKETRUM: ASIC IMPLEMENTATION

The replication of a general-purpose neuromorphic sensor using silicon technology is driven by its diverse applications

> REPLACE THIS LINE WITH YOUR MANUSCRIPT ID NUMBER (DOUBLE-CLICK HERE TO EDIT) <

in domains such as brain-computer interfaces (BCIs), cochlear implants, and portable devices requiring energy-efficient, real-time signal processing. These capabilities are particularly crucial for tasks like speech recognition on edge devices. The FPGA-based implementation of the Spiketrum system, detailed in Chapter II, was rigorously validated on a Xilinx Artix-7 FPGA. To achieve hardware and power efficiency, key storage components, such as Signal RAM and Time-Domain Kernel ROM (illustrated in Fig. 1-a), were designed for off-chip implementation.

This optimized design was subsequently converted into an Application-Specific Integrated Circuit (ASIC) using TSMC’s 180 nm process technology. The transformation leveraged Cadence’s Genus for RTL synthesis, targeting TSMC digital libraries. The resulting netlist was processed by Innovus, Cadence’s placement-and-routing (P&R) tool, which assigned physical locations to cells and routed interconnections, producing the final circuit layout. The design prioritized minimizing power consumption, reducing area, and meeting real-time signal processing requirements within strict timing constraints. The layout size was primarily determined by the number of I/O points, necessary for extensive prototype testing and verification.

The neuromorphic sensor chip utilizes TSMC’s 5M 1P CMOS 180 nm technology, with a compact die size of 4.4×4.4 mm, making it suitable for applications requiring minimal spatial footprints. Operating over a wide frequency range of 20 Hz to 8 kHz, the chip supports diverse signal processing needs. It provides an input dynamic range of 120 dB, enabling robust performance across varying signal strengths. With a supply voltage of 1.8 V and power consumption of just 63 mW, the chip achieves exceptional energy efficiency, suitable for power-sensitive environments. A comprehensive view of the layout is presented in Fig. 3.

Several optimization strategies were employed to achieve the desired performance metrics. Clock-gating cells were inserted to reduce dynamic power consumption. Hierarchical floorplanning grouped related modules to streamline routing and minimize interconnect delays. Pipeline registers were selectively placed to meet timing requirements at higher clock speeds, ensuring reliability for real-time applications. The design flow also incorporated iterative power and timing closure steps, guided by custom constraints to minimize switching activity and maintain functional margins. For high-speed paths intersecting large fan-out nets, dedicated buffers were added to ensure signal integrity, albeit with a slight area overhead.

The layout design utilized various TSMC libraries tailored for the 180 nm process. The tcb018gbwp7t library provided a comprehensive range of standard logic cells, including adders, multipliers, buffers, and flip-flops, forming the core logic. The tpd018bcdnv5 library supported I/O driver cells, including dual-driving I/O cells with enable-controlled pull-down resistors, core Vdd and GND pads, and I/O power supply pads. The tpv018v library was used for bond pads. These libraries ensured compliance with foundry design rules while limiting the design to available standard cells and pad configurations within TSMC’s 180 nm technology.

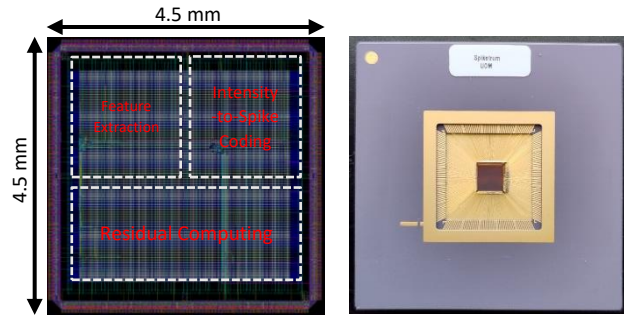


Fig. 3: A Photograph of the fabricated IC and an image of the layout of the proposed Spiketrum implementation.

Table I illustrates the characteristics of the IC of Spiketrum at different operating frequencies, highlighting significant differences in cell count, power consumption, and performance. At 200 MHz, the IC exhibits the highest cell count (4203) and power consumption (63.16 mW), achieving performance metrics of 3000 spikes per second and 9 spikes per segment. Reducing the clock speed to 50 MHz decreases the cell count to 3287 and significantly lowers power consumption to 13.16 mW, with performance metrics dropping to 750 spikes per second and 2 spikes per segment. These variations clearly illustrate the trade-offs between power consumption and performance across different clock speeds in the Spiketrum IC.

TABLE I: CHARACTERISTICS OF THE IC OF SPIKETRUM FOR VARIES OF OPERATING FREQUENCIES

Clock Speed		200 MHz	100 MHz	50 MHz
Cell Count (cell)		4203	3283	3287
Area (μm^2)		3,162	3,151	3,152
Power Consumption (mW)	Internal	42.83	18.34	9.28
	Switching	20.32	7.71	3.88
	Leakage	0.0006	0.0005	0.0005
	Total	63.16	26.05	13.16
Performance	Spike / Second	3000	1500	750
	Spike / Segment	9	4.5	2

IV. METHODOLOGY

In this chapter, we detail the methodologies employed to evaluate the proposed area-optimized FPGA-based Spiketrum design across two real-life applications: sound classification and ECG classification. The evaluation focused on assessing the performance of spiking and non-spiking neural network classifiers in terms of accuracy, computational efficiency, and training complexity.

To further optimize Spiketrum for ECG processing, we introduced a lightweight, power-efficient Multilayer Perceptron (MLP) model, designed in conjunction with the Temporal Averaging preprocessing technique. This combination leverages the temporal dynamics of ECG signals to reduce computational complexity while maintaining high classification performance. The analysis also included traditional deep learning models, such as Convolutional Neural Networks (CNNs) and Long Short-Term Memory networks (LSTMs), alongside neuromorphic counterparts,

> REPLACE THIS LINE WITH YOUR MANUSCRIPT ID NUMBER (DOUBLE-CLICK HERE TO EDIT) <

including Recurrent Spiking Neural Networks (RSNNs) and Adaptive Recurrent Spiking Neural Networks (aRSNNs), providing a comprehensive performance comparison.

The classification and evaluation results are presented in Chapter V, highlighting the efficacy of each model and preprocessing technique across the two application domains.

A. Classifier Models

We employed the same four classifiers for both tasks, including both non-spiking and spiking neural networks. This setup enabled us to evaluate performance in terms of accuracy, computational efficiency, and training complexity.

1) Non-Spiking Classifiers:

Convolutional Neural Network (CNN): The architecture starts with a Conv2D layer (32 filters, 11x11 kernel, ReLU activation), followed by a 3x3 MaxPooling2D and BatchNormalization layer. This pattern repeats with two additional Conv2D layers (3x3 kernel), followed by Flatten, a 128-unit fully connected layer with ReLU activation, and a SoftMax output layer for classification.

Long Short-Term Memory (LSTM): This model includes an input layer, an LSTM layer with 128 units, followed by global average pooling to reduce dimensionality. A 128-unit fully connected layer with ReLU activation is followed by dropout (rate = 0.5) and a SoftMax output layer for classification.

2) Spiking Classifiers:

Recurrent Spiking Neural Network (RSNN): Comprising two layers with 128 Leaky Integrate-and-Fire (LIF) neurons, this network has event-driven recurrent connections and is trained with Backpropagation Through Time (BPTT) using surrogate gradient descent, optimized by the Adamax algorithm.

Adaptive Recurrent Spiking Neural Network (aRSNN): Built similarly to the RSNN but with Adaptive Leaky Integrate-and-Fire (aLIF) neurons, this model leverages neuron adaptivity for enhanced performance. It uses categorical cross-entropy loss, also optimized by Adamax.

B. Preprocessing Techniques

Two preprocessing techniques were employed on the spike sequences:

Raw Spike Input Method: Directly feeds unprocessed spike sequences to classifiers.

Temporal Averaging Method: Computes the average spike activity over time per channel, resulting in a static 120-dimensional vector. This method reduces complexity, improving pattern learning and generalization, especially in ECG classification for enhancing QRS complex detection.

C. Optimized Model (Multilayer Perceptron, MLP)

A Multilayer perceptron (MLP) model was used with the Temporal Averaging Method to provide a lightweight, power-efficient solution. The MLP architecture includes an input layer for the 120-dimensional vector, followed by a hidden layer with 256 units (ReLU), a second hidden layer with 64 units, and a SoftMax output layer.

D. Model Training

Non-optimized Models (LSTM, CNN, RSNN, aRSNN): Models were trained with a batch size of 128 over 100 epochs, using a learning rate of 1e-2 for the LSTM, CNN, and RSNN, and 5e-4 for the aRSNN. Optimal performance was based on highest validation accuracy (Fig. 4-a) and epochs needed (Fig. 4-b).

Optimized Model (MLP): The MLP was trained with a batch size of 64, a learning rate of 1e-3, and a 10% reduction every 50 epochs over 400 epochs.

E. Datasets

ECG Classification: We used the 2017 PhysioNet/CinC Challenge dataset, containing single-lead ECG recordings categorized as Normal (N), Atrial fibrillation (A), Other rhythms (O), and Noisy signals (~). Data augmentation balanced the dataset by replicating A and N signals, resulting in 1,000 samples per class for training and 250 samples per class for testing.

Sound Classification: The Google Speech Commands (GSC2) dataset provided 6,000 samples of spoken digits for training and testing (5:1 ratio). Each digit was encoded by Spiketrum at 256 spikes per segment (5.885 kHz) and subsequently classified using spiking and non-spiking models.

F. Performance Metrics

To comprehensively evaluate the classification performance of both spiking and non-spiking models, we employed standard metrics, including precision, recall, and F1 score, alongside accuracy. These metrics provide deeper insights into the models' predictive reliability, especially in imbalanced datasets.

Precision (P): quantifies the proportion of correctly classified positive instances among all predicted positives, assessing the model's ability to minimize false positives:

$$P = \frac{TP}{TP + FP} \quad (6.2)$$

where TP represents true positives and FP denotes false positives.

Recall (R): measures the proportion of correctly identified positive instances among all actual positives, reflecting the model's ability to detect relevant patterns:

$$R = \frac{TP}{TP + FN} \quad (6.3)$$

where FN represents false negatives.

F1 Score provides a harmonic mean of precision and recall, balancing both metrics to account for trade-offs between false positives and false negatives:

$$F1 = 2 \frac{P \times R}{P + R} \quad (6.4)$$

These metrics ensure a rigorous assessment of classifier performance across different spike rates and classification tasks. A high F1 score indicates a well-balanced model, particularly in cases where class distributions are uneven. The results, including accuracy and training efficiency, are further analysed in Chapter V.

> REPLACE THIS LINE WITH YOUR MANUSCRIPT ID NUMBER (DOUBLE-CLICK HERE TO EDIT) <

V. EXPERIMENTAL RESULTS OF REAL-LIFE APPLICATIONS

This chapter evaluates the performance of the classifiers across ECG and sound classification tasks, examining trade-offs between spiking and non-spiking models and demonstrating Spiketrum’s versatility in practical applications.

A. ECG Classification

1) Classification Results:

Among the non-spiking models, LSTM achieved the highest accuracy, consistently exceeding 80% across most spike rates. It reached peak accuracy of approximately 88% at 512 spikes per second (sps), requiring fewer than 30 epochs for convergence. However, the LSTM exhibited higher variability in training performance across different spike rates, suggesting sensitivity to spike distribution patterns. The CNN, while competitive, performed slightly below the LSTM, achieving around 87% accuracy at 512 sps.

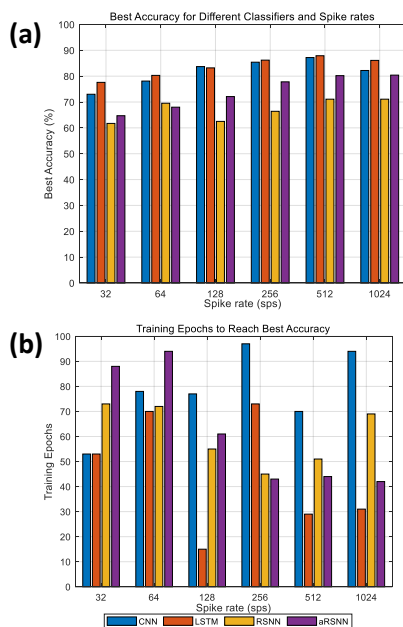


Fig. 4: Classification accuracy and training time analysis of the Spiketrum at different spike rates (Spikes Per Segment, sps unit is used, and the segment size is 43.5 ms) for spiking and non-spiking classifiers. (a) illustrates the maximum classification accuracy on the test dataset after 100 epochs of training for Convolutional Neural Networks (CNNs), Long Short-Term Memory (LSTM), Recurrent Spiking Neural Network (RSNN), and Adaptive Recurrent Spiking Neural Network (aRSNN). (b) illustrates the number of epochs required to achieve the maximum accuracy across various spike rates. These results are based on the analysis performed using the 2017 PhysioNet/CinC Challenge dataset.

Unlike the LSTM, the CNN required more training epochs to achieve effective convergence, especially at higher spike rates. These differing training requirements highlight the trade-off between the CNN’s learning efficiency and its ability to generalize across varied spike rates. For spiking models, the RSNN demonstrated fluctuating performance, achieving a maximum accuracy of approximately 71% at 512 sps. However, it required around 52 epochs for convergence,

indicating slower training dynamics compared to the non-spiking models.

In contrast, the aRSNN, which incorporates adaptive dynamics, displayed superior performance among spiking models, reaching nearly 80% accuracy at 512 sps. The aRSNN also exhibited more stable training behaviour, with accuracy consistently increasing as the spike rate increased. Additionally, it required fewer epochs to converge at higher spike rates compared to the RSNN, making it a more efficient and robust spike-based classifier, as its adaptive mechanisms optimize learning efficiency by better leveraging increased spike activity for faster weight updates and improved stability. These results highlight the differing sensitivities of spiking and non-spiking models to spike rate configurations. Non-spiking models, particularly the LSTM, leverage their sequential processing capabilities to achieve high accuracy but require careful training parameter tuning to avoid variability. Spiking models, while generally less accurate, demonstrate promise for energy-efficient applications, with the aRSNN emerging as the most robust and adaptable classifier due to its ability to optimize learning across varying spike rates with stable and efficient training dynamics.

2) Performance Evaluation

During testing, each model’s performance was evaluated on the test set at the optimal spike rate identified during training. Precision, recall, and F1 score were used to assess generalization, with results summarized in Table II.

TABLE II: PRECISION, RECALL, AND F1 SCORE COMPARISON OF SPIKING AND NON-SPIKING CLASSIFIERS FOR ECG CLASSIFICATION

Classifiers	Precision (%)	Recall (%)	F1 Score (%)
LSTM	85.29	85.63	85.30
CNN	78.56	78.5	77.29
RSNN	54.30	53.0	53.64
aRSNN	64.10	63.8	63.95

The table highlights significant differences in classification performance among the evaluated models. The LSTM classifier achieves the highest F1 score (85.30%), outperforming the CNN by over 10%, demonstrating strong predictive accuracy with well-balanced precision and recall. While the CNN follows closely, its slight imbalance between precision (78.56%) and recall suggests a higher tendency for misclassifications in certain cases.

Among the spiking models, the aRSNN outperforms the RSNN across all metrics, achieving an F1 score of 63.95%, which is around 10% higher than the RSNN’s 53.64%. This improvement highlights the benefit of adaptive dynamics in enhancing classification accuracy. However, both spiking models show significantly lower scores compared to non-spiking models, with the RSNN exhibiting the weakest performance, particularly in recall (53.0%), suggesting a tendency to miss positive instances more frequently.

Overall, the results emphasize the superior classification capability of non-spiking models, particularly the LSTM, while demonstrating the potential of adaptive spiking networks in narrowing the performance gap. The lower F1 scores of RSNN and aRSNN indicate that further optimizations, such as architectural enhancements or

> REPLACE THIS LINE WITH YOUR MANUSCRIPT ID NUMBER (DOUBLE-CLICK HERE TO EDIT) <

improved training strategies, may be necessary to enhance their predictive reliability.

3) ECG Optimization

The temporal averaging method, combined with a Multilayer Perceptron (MLP) classifier, was introduced as a lightweight, power-efficient approach for ECG classification, as detailed in the Methodology chapter. This method was designed to reduce computational complexity while maintaining high classification performance, making it suitable for real-time and resource-constrained applications.

In this chapter, we evaluate the effectiveness of this optimization by comparing it with conventional deep learning and spiking models using the raw spike input method. The evaluation considers computational complexity, accuracy, and F1 score. The results highlight the advantages of temporal averaging with MLP, demonstrating significantly lower computational demands while achieving superior classification performance compared to both non-spiking and spiking neural networks.

As shown by Table III, the temporal averaging method, combined with an MLP classifier, achieves the highest accuracy of 93.27% and the best F1 score of 93.75%, while requiring only 95,364 MACs (Multiply-Accumulate Operations). This demonstrates that temporal averaging significantly reduces computational demands while enhancing classification performance, making it a highly efficient approach for resource-constrained environments.

TABLE III: COMPUTATIONAL COMPLEXITY AND CLASSIFICATION PERFORMANCE OF SPIKING AND NON-SPIKING MODELS FOR ECG AT 256 SPS

Preprocessing Method	Classifier (256 sps)	computational complexity (MACs)	Accuracy (%)	F1 Score (%)
Temporal Averaging	MLP	95,364	93.27	93.75
Raw Spike Input	LSTM	4,797,696	85.50	85.42
	CNN	6,226,944	80.62	77.29
	RSNN	9,932,800	51.95	63.40
	aRSNN	11,593,670	63.95	51.40

The raw spike input method significantly increases computational complexity across classifiers. While the LSTM and CNN models achieve competitive accuracy (85.50% and 80.62%, respectively), they require 4.8 million and 6.2 million MACs, making them computationally expensive compared to the MLP. The spiking classifiers, RSNN and aRSNN, demand even higher complexity (9.93 million and 11.59 million MACs, respectively) but achieve the lowest accuracy, with aRSNN improving over RSNN by 12%. Their lower F1 scores suggest inconsistent performance across classes, highlighting a trade-off between biological relevance and classification effectiveness.

Overall, the results indicate that the combination of temporal averaging and MLP provides the best balance between computational efficiency and classification accuracy. While deep learning models like LSTM and CNN perform well, their higher computational cost makes them less efficient. The spiking networks, although promising for neuromorphic applications, require further optimization to

close the performance gap with non-spiking models.

B. Sound Classification

1) Classification Results

CNNs achieve consistently high accuracy across all spike rates, exceeding 75% in most cases, with peak accuracy observed at 256 and 512 sps. However, they require a greater number of training epochs at lower spike rates. At 32 sps, CNN training exceeds 95 epochs, whereas at 512 sps, it converges in approximately 60 epochs, illustrating a clear trade-off between training time and spike rate. This behaviour reflects the CNN's dependence on higher spike rates for efficient feature extraction and convergence.

LSTMs maintain stable accuracy across all spike rates, surpassing 85% at 128, 256, and 512 sps. They require a moderate number of training epochs, with convergence times peaking at 72 epochs at 64 sps. Unlike CNNs, LSTMs demonstrate less sensitivity to spike rate variations, making them more adaptable across different input configurations. Their ability to capture long-term dependencies in sequential data contributes to their robust performance in sound classification tasks.

Spiking models exhibit greater sensitivity to spike rate variations, highlighting the challenges of spike-based learning. The RSNN achieves its highest accuracy at 256 sps but performs poorly at lower rates, with accuracy dropping below 50% at 32 and 64 sps, indicating limited generalization in low-spike-rate scenarios. While it converges relatively quickly at 128 sps, requiring around 40 epochs, it demands significantly more training time at other rates, reflecting inefficiencies in adapting to varying spike densities.

The aRSNN improves upon the RSNN, achieving nearly 55% accuracy across all spike rates. However, it requires more training epochs as the spike rate increases, particularly at 256 and 512 sps, where its convergence time matches or exceeds that of the RSNN. Despite its adaptive dynamics offering better stability and accuracy than the RSNN, the aRSNN still struggles to generalize effectively at lower spike rates, where spike-based learning is inherently more challenging.

At lower spike rates (32 and 64 sps), all classifiers, particularly spiking models, exhibit suboptimal performance, indicating a need for careful tuning or alternative preprocessing strategies to enhance learning in low-density spike scenarios. Mid-range spike rates (128 and 256 sps) provide a better balance between accuracy and training efficiency, particularly for LSTMs and CNNs, which leverage these rates to achieve stable performance with manageable training times.

Overall, LSTMs emerge as the most versatile classifier, offering a reliable balance of accuracy and training efficiency across all spike rates. Their ability to process sequential data and capture long-term dependencies makes them particularly suited for sound classification tasks. In contrast, RSNNs and aRSNNs, while capable of faster convergence at specific spike rates, require careful tuning to mitigate performance weaknesses at low spike rates. These results underscore the importance of selecting an appropriate classifier based on the computational constraints and accuracy requirements of the

> REPLACE THIS LINE WITH YOUR MANUSCRIPT ID NUMBER (DOUBLE-CLICK HERE TO EDIT) <

target application, with non-spiking models being more robust and adaptable to varied spike configurations, while spiking models may find utility in energy-constrained scenarios with further optimization.

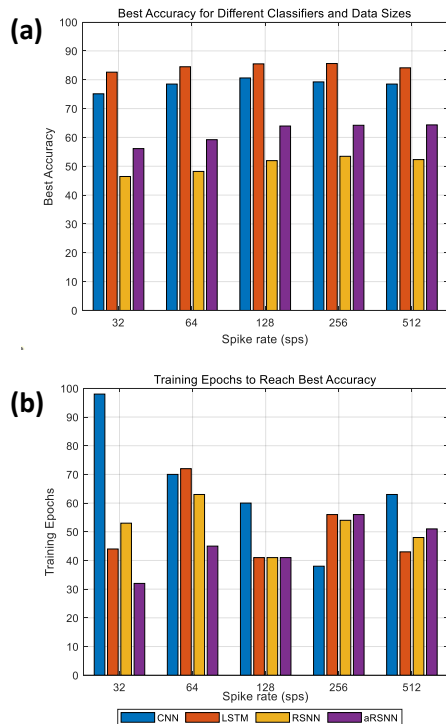


Fig. 5: A comprehensive comparison of the training performance of the various non-spiking and spiking classifiers across different spike rates. (a) illustrates the highest accuracy percentages achieved by each classifier at varying spike rates, demonstrating a clear relationship between classifier performance and spike rate. Meanwhile, (b) shows the number of training epochs required to reach the best accuracy, offering insights into the training efficiency of each classifier under different spike rate conditions.

TABLE IV: PERFORMANCE METRICS OF SPIKING AND NON-SPIKING CLASSIFIERS FOR SOUND CLASSIFICATION AT DIFFERENT SPIKE RATES

Spike rate	Classifier	Precision %	Recall %	F1 Score %
128	CNN	81.90	80.4	80.36
	LSTM	79.16	78.6	78.50
	RSNN	59.09	58.9	58.84
	aRSNN	72.10	72.0	71.88
256	CNN	84.52	84.3	84.28
	LSTM	84.92	83.8	83.76
	RSNN	63.40	62.6	63.0
	aRSNN	76.54	76	76.01

2) Performance Evaluation:

This chapter evaluates the performance of non-spiking (CNN and LSTM) and spiking (RSNN and aRSNN) classifiers for sound classification at different spike rates. The analysis focuses on metrics such as precision, recall, and F1 score to provide a comprehensive understanding of the models' classification capabilities. Table IV compares the performance of various classifiers for sound classification at two spike rates, 128 and 256 spikes per second (sps), using precision, recall, and F1 score.

At 128 sps, the CNN achieves the highest F1 score

(80.36%), followed closely by the LSTM at 78.50%. Both non-spiking models demonstrate strong performance in precision and recall, with the CNN slightly leading in precision (81.90%). In contrast, spiking models perform less effectively, with the aRSNN achieving an F1 score of 71.88% and the RSNN lagging behind at 58.84%, highlighting the limitations of spiking models at lower spike rates despite some improvements in adaptivity with the aRSNN.

At 256 sps, all classifiers see performance gains. The LSTM slightly surpasses the CNN, achieving the highest F1 score (83.76%) and precision (84.92%), while the CNN closely follows with an F1 score of 84.28%. The aRSNN also improves significantly at the higher spike rate, reaching an F1 score of 76.01% compared to 71.88% at 128 sps, demonstrating its sensitivity to spike rate configurations. However, the RSNN remains the weakest performer, with an F1 score of 63.0%.

These results indicate that non-spiking models, particularly the LSTM and CNN, consistently outperform spiking models in both precision and recall. Still, the aRSNN shows promise for improvement at higher spike rates, reducing the gap between spiking and non-spiking models.

VI. DISCUSSION

This study presents an area-optimized implementation of a general-purpose spike encoder using the Spiketrum algorithm. Building on our previous work, which introduced a high-throughput, performance-optimized version for parallel-processing architectures such as FPGAs [12], this chapter expands on Spiketrum's practical utility by comparing both implementations across dimensions like spike generation time, rate, power consumption, resource usage, and practical applicability. This comparative analysis provides insights to support informed decisions for diverse application needs, with benchmarking conducted on an FPGA for consistency. Notably, these results can guide users in selecting the optimal hardware—whether FPGA, ASIC, or others—for their specific requirements.

The area-optimized implementation, which employs time-domain convolution, achieves a spike generation time of 4.7 ms, producing up to 9 spikes per segment (equivalent to 206 spikes per second). Using only 3 DSP slices, 96 BRAMs, and 1,704 LUTs, this design achieves significant resource efficiency. However, its reduced spike generation rate limits its suitability for high-frequency requirements, though it remains effective for applications that prioritize low power usage. The implementation's total power consumption is 365 mW, underscoring its suitability for energy-sensitive applications while still allowing room for optimization in throughput.

In contrast, the performance-optimized version, leveraging frequency-domain convolution, achieves a notably fast spike generation time of 0.5 ms, generating up to 80 spikes per segment (or 3,000 spikes per second). This implementation's performance comes at the cost of significantly higher resource usage—235 DSP slices (a more than 7,700% increase), 285 BRAMs (nearly 196% increase), and 8,756 LUTs (over 413% increase)—positioning it for tasks that demand substantial computational power and high-speed

> REPLACE THIS LINE WITH YOUR MANUSCRIPT ID NUMBER (DOUBLE-CLICK HERE TO EDIT) <

processing. Its power consumption, totalling 1.3 W with 89% attributed to dynamic power, signals challenges for use in energy-constrained environments, though its rapid spike generation is well-suited for high-speed real-time processing tasks.

Table V compares Spiketrum’s FPGA implementations with other spike encoders from the literature, emphasizing differences in power efficiency, resource utilization, and throughput.

The audio-processing encoder in [18] consumes 1,260 mW, which is 3.17% lower than Spiketrum’s 1,382 mW performance-optimized implementation but significantly higher than the area-optimized version (365 mW, a 71.03% reduction). Despite its lower power consumption compared to the performance-optimized Spiketrum, its throughput remains unspecified, making direct efficiency comparisons challenging. Additionally, this encoder uses 49 DSP slices, which is 79.15% lower than Spiketrum’s 235 DSPs, but 63.27% higher than Spiketrum’s area-optimized implementation (3 DSPs). In terms of LUT utilization, it consumes 5,235 LUTs, 40.2% fewer than Spiketrum’s performance-optimized version but 207.2% more than Spiketrum’s area-optimized design. With a RAM usage of 571 kB, it requires 11.04% less than Spiketrum’s performance-optimized version and 164.35% more than the area-optimized implementation.

The ECG-optimized encoder in [19] is highly power-efficient, consuming just 28 mW, making Spiketrum’s power consumption 4,835.7% higher (performance-optimized version) and 1,203.6% higher (area-optimized version). However, this efficiency comes at the cost of extremely low throughput (3 beats per second), while Spiketrum achieves a 99,900% increase in throughput (3,000 sps). Resource utilization also reflects this tradeoff: Spiketrum’s performance-optimized version uses 1,019.05% more DSPs (235 vs. 21) but reduces LUT usage by 55.47%, using 8,756 LUTs instead of 19,663 LUTs. RAM usage is significantly higher in Spiketrum (642 kB, a 1,184% increase), as its broader application scope demands larger memory buffers.

The EMG-based encoder in [20] is highly resource-intensive, consuming 498 DSP slices and 90,683 LUTs, yet achieving only 2 samples per second. In comparison, Spiketrum reduces DSP usage by 52.81% and LUT usage by 90.34%, while providing a 149,900% increase in throughput, demonstrating its superior efficiency in high-speed processing. RAM usage is 2,894 kB, which is 350.86% higher than Spiketrum’s performance-optimized version, reflecting the EMG encoder’s reliance on extensive memory resources.

Compared to alternative designs, Spiketrum offers significant advantages in power efficiency and flexible control over spike rates, making it adaptable to a wide range of sensory input applications. This flexibility makes Spiketrum a versatile solution for diverse application domains. The area-optimized implementation is particularly suited for applications requiring a balance between low resource consumption and moderate real-time processing, such as low-power neural networks and sensor data processing, where computational and power efficiency are critical. On the other hand, the performance-optimized

version excels in high-speed, real-time signal processing tasks, including real-time audio recognition, where rapid spike generation and high throughput are essential.

TABLE V: A COMPARISON OF SPIKETRUM IMPLEMENTATIONS WITH OTHER ENCODERS FOUND IN LITERATURE.

	Spiketrum Performance-Optimized	Spiketrum Area-Optimized	Spiketrum IC	[18]	[19]	[20]
Year	2025			2018	2021	2023
Tech	Xilinx Artix-7		TSMC 180	Altera Cyclone-5	Xilinx Artix-7	Xilinx Kintex UltraScale+
Power (mW)	1382	365	63	1260	28	-
DSP	235	3		49	21	498
LUTs	8756	1704		5235	19,663	90683
RAMs (kB)	642	216		571	50	2894
Throughput	3000 sps	206 sps		-	3 beats/s	2 samples/s
Application	General Purpose			Audio	ECG	EMG

The choice between these implementations depends on the specific computational demands and resource constraints of the target application. For tasks requiring minimal power and area, the Spiketrum IC implementation is the most suitable option. It achieves an optimal balance between energy efficiency and compact design, making it ideal for energy-sensitive environments and applications with strict area constraints. Meanwhile, the performance-optimized FPGA implementation is better suited for high-performance scenarios, where speed and precision outweigh power and area limitations.

While the IC implementation incorporates a variety of optimization techniques, certain limitations persist. The use of the 180 nm process technology, although robust and well-established, lacks the power efficiency and higher transistor density available in more advanced nodes, such as 7 nm or 5 nm technologies. Transitioning to these smaller process nodes could further improve power efficiency and compactness. Additionally, off-chip storage for Signal RAM and Time-Domain Kernel ROM effectively reduces on-chip area requirements but introduces potential latency and bandwidth bottlenecks, particularly in high-throughput scenarios. Furthermore, the inclusion of numerous I/O pins, driven by testing and verification requirements, limits layout efficiency and increases the chip’s overall footprint.

Despite these challenges, the selected technology and design approach strike a practical balance between feasibility, reliability, and cost-effectiveness. The Spiketrum IC implementation, with its compact die size and low power consumption, is particularly well-suited for prototyping and low-to-medium volume production, while maintaining the adaptability to address a variety of neuromorphic and signal

> REPLACE THIS LINE WITH YOUR MANUSCRIPT ID NUMBER (DOUBLE-CLICK HERE TO EDIT) <

processing challenges across diverse application domains.

VII. CONCLUSION

In conclusion, we have presented an area-optimized FPGA-based implementation of a general-purpose spike-based encoder. The proposed implementations were implemented and verified through various applications, including audio processing and bio-signal processing (ECG and EMG classification). An ASIC implementation of the proposed design was also developed and sent for fabrication. Future work will include comprehensive testing and verification of the proposed implementations with a variety of real-life applications. Additionally, we plan to test and verify the functionality of the designed ASIC in real-life scenarios, such as robotics-based applications.

REFERENCES

- [1] G. S. Rose, M. S. A. Shawkat, A. Z. Foshie, J. J. Murray, and M. M. Adnan, "A system design perspective on neuromorphic computer processors," *Neuromorphic Computing and Engineering*, vol. 1, no. 2, p. 022001, 2021.
- [2] C. D. Schuman, J. S. Plank, G. Bruer, and J. Anantharaj, "Non-traditional input encoding schemes for spiking neuromorphic systems," in *2019 International Joint Conference on Neural Networks (IJCNN)*, 2019: IEEE, pp. 1-10.
- [3] X. Qi, X. Guo, and J. G. Harris, "A time-to-first spike CMOS imager," in *2004 IEEE International Symposium on Circuits and Systems (ISCAS)*, 2004, vol. 4: IEEE, pp. IV-824.
- [4] C. Shoushun and A. Bermak, "Arbitrated time-to-first spike CMOS image sensor with on-chip histogram equalization," *IEEE Transactions on Very Large Scale Integration (VLSI) Systems*, vol. 15, no. 3, pp. 346-357, 2007.
- [5] Y. Yi *et al.*, "FPGA based spike-time dependent encoder and reservoir design in neuromorphic computing processors," *Microprocessors and Microsystems*, vol. 46, pp. 175-183, 2016.
- [6] S. M. Bohte, J. N. Kok, and H. La Poutre, "Error-backpropagation in temporally encoded networks of spiking neurons," *Neurocomputing*, vol. 48, no. 1-4, pp. 17-37, 2002.
- [7] C. Liu *et al.*, "A spiking neuromorphic design with resistive crossbar," in *Proceedings of the 52nd Annual Design Automation Conference*, 2015, pp. 1-6.
- [8] A. Bagheri, O. Simeone, and B. Rajendran, "Training probabilistic spiking neural networks with first-to-spike decoding," in *2018 IEEE International Conference on Acoustics, Speech and Signal Processing (ICASSP)*, 2018: IEEE, pp. 2986-2990.
- [9] D. Querlioz, O. Bichler, and C. Gamrat, "Simulation of a memristor-based spiking neural network immune to device variations," in *The 2011 International Joint Conference on Neural Networks*, 2011: IEEE, pp. 1775-1781.
- [10] C. Schuman, C. Rizzo, J. McDonald-Carmack, N. Skuda, and J. Plank, "Evaluating encoding and decoding approaches for spiking neuromorphic systems," in *Proceedings of the International Conference on Neuromorphic Systems 2022*, 2022, pp. 1-9.
- [11] P. G. Huajin Tang, Jayawan Wijekoon, MHD Anas Alsakkal, Ziming Wang, Rui Yan, "Neuromorphic Auditory Perception by Neural Spiketrum," *IEEE Transactions on Emerging Topics in Computational Intelligence* 2025, doi: 10.1109/TETCI.2024.3419711.
- [12] M. A. Alsakkal and J. Wijekoon, "Spiketrum: An FPGA-Based Implementation of a Neuromorphic Cochlea," *IEEE Transactions on Circuits and Systems*, 2025, doi: 10.1109/TCSI.2025.3526585.
- [13] S. G. Mallat and Z. J. I. T. o. s. p. Zhang, "Matching pursuits with time-frequency dictionaries," vol. 41, no. 12, pp. 3397-3415, 1993.
- [14] R. M. Bittner, J. Salamon, M. Tierney, M. Mauch, C. Cannam, and J. P. Bello, "Medleydb: A multitrack dataset for annotation-intensive mir research," in *ISMIR*, 2014, vol. 14, pp. 155-160.
- [15] T. Feist, "Vivado design suite," *White Paper*, vol. 5, p. 30, 2012.
- [16] A. Finnerty and H. Ratigner, "Reduce power and cost by converting from floating point to fixed point," *WP491 (v1.0)*, 2017.
- [17] Xilinx, "7 Series DSP48E1 Slice User Guide," 2018. [Online]. Available: https://docs.xilinx.com/v/u/en-US/ug479_7Series_DSP48E1
- [18] Y. Xu, C. S. Thakur, R. K. Singh, T. J. Hamilton, R. M. Wang, and A. Van Schaik, "A FPGA implementation of the CAR-FAC cochlear model," *Frontiers in neuroscience*, vol. 12, p. 198, 2018.
- [19] M. P. Desai, G. Caffarena, R. Jevtic, D. G. Márquez, and A. Otero, "A low-latency, low-power FPGA implementation of ECG signal characterization using hermite polynomials," *Electronics*, vol. 10, no. 19, p. 2324, 2021.
- [20] H.-S. Choi, "Electromyogram (EMG) signal classification based on light-weight neural network with FPGAs for wearable application," *Electronics*, vol. 12, no. 6, p. 1398, 2023.